Nongeometrical S^* arrival in a transversely isotropic solid

Lawrence H. T. Le and E. S. Krebes

ABSTRACT

A complete solution based on wavenumber-frequency $(\omega\text{-}k)$ method for a buried point source in a homogeneous transversely isotropic elastic or anelastic half-space is presented. By means of the method of steepest descent, a high frequency approximation to the nongeometrical S^* wave in a weakly anisotropic elastic half-space is also developed. Full-wave synthetic seismograms with a buried vertical point force and an explosive point source show the existence of the S^* arrival in the anisotropic Austin Chalk (weakly anisotropic) and Gypsum Soil (strongly anisotropic). However, the nongeometrical S^* arrival is much more prominent in the weakly anisotropic solid than in the strongly anisotropic solid.

INTRODUCTION

In a numerical experiment to a perfectly elastic, homogeneous, isotropic half-space problem, Hron and Mikhailenko (1981) detected a strong nongeometrical arrival S^* for an explosive point source buried shallowly below the free surface. The existence of the S^* arrival is prominent when the source depth is less than one wavelength and the angle ϕ which the S^* ray makes with the free surface is greater than $\phi^* = \sin^{-1}(\beta/\alpha)$ where α and β are, respectively, the phase velocities of the compressional and shear waves in the isotropic half-space. The S^* wave was interpreted physically to be generated at the free surface above the source due to the interaction between the free surface and the inhomogeneous waves making up the spherical compressional wavefronts radiated by the source. The S^* wave, propagating with a shear wave speed of the isotropic solid, possesses most of the characteristics of a body wave, e.g., linear polarization, transverse particle motion (Daley and Hron, 1983a) and are, therefore, subject to reflection and transmission at the interface (Daley and Hron, 1983b).

Hron and Mikhailenko (1981) associated the S^* arrival with a secondary saddle-point contribution to the integral representing the reflected shear wave from the free surface. Daley and Hron (1983a) later derived a saddle-point approximation to the S^* arrival in a half-space and further extended the development to a transmission problem of two perfectly elastic, homogeneous, isotropic half-spaces (Daley and Hron, 1983b). In recent years, the existence of the S^* wave has been favorably supported by field data (Gutowski et al., 1984) and experimental data of physical modeling (Kim and Behrens, 1986).

Transverse isotropy (TI) with a vertical axis of symmetry assumes azimuthal isotropy and is commonly observed in sedimentary basins consisting of shale-like or clay-like layers. Unlike in isotropic medium, phase velocity and ray velocity at which energy propagates are different and depend on direction in TI medium (Figure 1). Wave surface is an important concept in TI medium. Especially in severe anisotropic

solid, *SV* wave surface has cusps and triplications indicating multiple arrivals at a particular direction. Measurements from borehole seismic (Uhrig and Van Melle, 1955; White et al., 1983) have shown that the wave speeds in the horizontal direction can be 20-40% higher than along the vertical direction. Studies of wave propagation in the TI solid are abundant (Stoneley, 1949; Postma, 1955; Backus, 1962; Crampin and Taylor, 1971; Daley and Hron, 1977; Sprenke and Kanasewich, 1977; Berryman, 1979; White, 1982; Byun, 1984; Helbig, 1984; Levin, 1989; Schoenberg, 1993; Krebes and Le, 1993). Perhaps, the first report on the observation of the presence of cusps in field data was presented by Slater et al. (1993) in their study of a uniformly plane layered clay reservoir in the Juravskoe oil field in Russia.

Shear wave such as the S^* is extremely useful to investigate the anisotropic effects. Martynov and Mikhailenko (1984) used a hybrid method combining integral transform and finite-difference to solve a wave propagation problem in an inhomogeneous transversely isotropic half-space due to a point source including an explosion; however, no obvious example was given to demonstrate the existence of the S^* wave. In this paper, we extend the investigation of the S^* wave to a homogeneous, transversely isotropic half-space. The wavefronts in a transversely isotropic solid are curved but not spherical and an explosion produces both the *quasi-compressional* (*qP*) and *quasi-shear* (*qS*) waves (Stoneley, 1949; White, 1982; Martynov and Mikhailenko, 1984; Abramovici and Le, 1993). A numerical investigation on S^* wave in a homogeneous transversely isotropic half-space will be presented. This is followed by deriving a high frequency approximation to the S^* wave in a weakly anisotropic elastic half-space. A complete wavenumber-frequency (ω-k) solution to the Lamb's problem provided in the Appendix will conclude the paper.

DISCUSSION OF NUMERICAL RESULTS

We consider a vertical point force acting within a homogeneous TI half-space. The homogeneous TI medium is an Austin Chalk. The phase and group velocities of Austin Chalk are shown in Figures 3a-b. The anisotropy factor (*AF*) measured by

$$AF\,[f(\gamma)] = \frac{f(\gamma) - f(\gamma{=}0)}{f(\gamma) + f(\gamma{=}0)} \times 100\% \tag{1}$$

(Carcione, 1992), where γ is either the phase or group angle from the symmetry axis (Figure 1) and f is the corresponding phase or group velocity function, is displayed in Figures 3c-d. The source function $g(t)$ used to compute the synthetic displacement seismograms is a first time derivative of a Gaussian function (Abramovici, Le and Kanasewich, 1989). The dominant frequency used is 35 Hz and dominant vertical *qP* wavelength λ is 72 m. Minor attenuation (Q = 400) is also applied. Elastic results can be simulated, if desired, by using the complex frequency technique (Mallick and Frazer, 1987).

The effect of source depth on the generation of the S^* wave is shown in Figure 4. A single receiver is placed at an offset of 12λ and a depth of 3λ. The source depth ranges from 0.1λ to 0.7λ. Only *qP* and converted reflection *qP*-*qS* are computed. The S^* wave is stronger at shallow source depth and has larger vertical than horizontal

amplitudes. As the source depth increases, the S^* arrival decays rapidly and disappears after 0.3 λ in the horizontal motion. Rayleigh wave is visible after the S^* arrival at h = 0.1 – 0.2 λ. Next we place a source at 0.1λ deep and a receiver at a fixed offset of 12λ but vary the receiver depth from 0 λ to 7 λ. The vertical and horizontal motions are shown in Figure 5. At shallow receiver depth, Rayleigh wave dominates and follows closely the S^* wave, producing a complex waveform of high amplitude. Rayleigh wave becomes separated from the S^* wave at z = 3 λ where the horizontal motion changes polarity around 0.83 s. From $z = 3\lambda$ onwards, the amplitude of the S^* wave increases with depth. Figure 6 shows the response of an array of receivers at a depth of 3 λ. The source is buried 0.1 λ deep and the offset starts from 1 λ to 16 λ. The S^* wave separates itself from the converted reflection $qPqS$ around 6 λ corresponding to a ray angle of 63.4°. The vertical motion of the S^* wave is much stronger than the $qPqS$ arrival and persists its existence throughout the offset range. The S^* wave is subject to reflection, transmission and mode conversion if an interface is encountered.

Radiation pattern of the S^* wave can be synthesized from the vertical s_z and horizontal s_r displacements based on the following rotational operation:

$$U_R = s_r \sin(\phi) + s_z \cos(\phi)$$

$$U_T = s_r \cos(\phi) - s_z \sin(\phi) \qquad (2)$$

where U_R and U_T are the radial and transverse displacements and ϕ is the ray angle. Note that both U_R and U_T are confined in the saggital plane (a vertical plane containing the source and the receivers). We place nine receivers evenly around a circular arc starting at 5° from the vertical axis. The radius of the arc is 13 λ and the center, where the vertical point force is located, is 0.1 λ from the free surface. Figure 7 shows the synthetic radiation pattern of the S^* wave. The polarization vector of the S^* wave has both the radial and transverse components but the latter is stronger. The converted $qPqS$ wave merges with the S^* arrival around 35°. The S^* wave exists in a region bounded below by a *distinct* or *critical* angle. At angles smaller than the distinct angle, the S^* wave does not exist. The distinct angle can be approximately obtained by finding the angle at which the reflected $qPqS$ wave and S^* wave meet. In this case, 35° is a good estimate. Rayleigh wave is visible at 85° in the transverse motion. Superimposed on the arrival is the arrival time of the direct qS arrival from the source. At small offset and large depth, the qP leg of the raypath for the converted $qPqS$ arrival is insignificant since the source depth is shallow and the arrival time can be approximated by the qS arrival. Also around this range, the distinct angle is not reached and the S^* arrival is not present. However, at large offset where the distinct angle is reached, the qP leg of the raypath for the S^* wave is negligible and thus the arrival can be determined approximately by the qS arrival time. Figure 8 shows the radiation pattern of the S^* wave for the same model configuration but with an explosive point source. The source function in this case is a second time derivative of a Gaussian function. The S^* wave is visible in both components.

Finally, we consider a strongly anisotropic solid, Gypsum Soil. The phase and group velocities are given in Figure 9. The dominant vertical qP wavelength in

Gypsum Soil is 54 m. Note that the wave surface of qS wave has cusps and triplication indicating multiple arrivals between 15° to 75° of ray angles. Figures 10 and 11 show the radiation patterns of the S^* arrival for the vertical point force and an explosive source. Attempt to find the distinct angle where the converted $qPqS$ wave and the S^* wave meet is difficult. However, it is fairly confident to say that at small ray angles, the $qPqS$ arrival is present and at large ray angles, the arrival is the S^* wave. The nongeometrical arrival is strong within a very narrow range above 60°. The high amplitude at 75° is due to the merging of two separate S^* arrivals at the cusp. The nongeometrical arrival at 85° is not predicted by the simple ray theory. As a comparison with the results in Austin Chalk, the nongeometrical S^* arrival generated by the free surface of Gypsum Soil is weaker. Rayleigh wave seems to be absent in Gypsum Soil but it is not conclusive since only the $qPqS$ term is computed. The contribution to the amplitude of the Rayleigh wave also comes from the other terms of, say, (A.9).

S* RAY IN A WEAKLY TRANSVERSELY ISOTROPIC SOLID

In the following, we consider the S^* wave generated by a point source buried at a shallow depth h below the free surface. The solid is a homogeneous transversely isotropic half-space with a vertical axis of azimuthal symmetry. The medium is a weakly anisotropic medium, whose qS slowness surfaces are convex, i.e., no cusps or triplications exist on the qS wave surfaces. Similar to its isotropic counterpart (Daley and Hron, 1983a), the S^* arrival in a transversely isotropic solid can be obtained by a secondary saddle-point approximation of the full wavefield of the reflected qP-qS wave. For $z > h$ and a monochromatic frequency ω, the vertical and horizontal displacements of the qP-qS reflection are (see Appendix A) :

$$s_z(r,z,t) = \frac{1}{2\pi} \mathrm{Re} \int_0^\infty Q(k)\, k\; e^{i\omega t - \zeta_{qP} h - \zeta_{qS} z} J_0(kr)\, dk \tag{3}$$

and

$$s_r(r,z,t) = \frac{1}{2\pi} \frac{\partial}{\partial r} \mathrm{Re} \int_0^\infty \frac{Q(k)}{k} \frac{B_{qS}}{\zeta_{qS}} J_0(k\,r)\, e^{\,i\,\omega t - \zeta_{qP} h - \zeta_{qS} z}\; dk \tag{4}$$

where $Q(k)$ characterizes the strength of the source and the qP-qS reflection coefficient:

$$Q(k) = -\, a_1(k)\, \boldsymbol{R}_{qPqS}\, \zeta_{qS}\,. \tag{5}$$

In order to evaluate s_z, we represent J_0 by the zeroth order Hankel function of the second kind. For $kr >> 1$, the Hankel function is asymptotically given by (Abramowitz and Stegun, 1972):

$$H_0^{(2)}(kr) \sim \sqrt{\frac{2}{\pi k r}}\, e^{-i\left(kr-\frac{\pi}{4}\right)} \quad . \tag{6}$$

With (6) and the following substitutions

$$k = \omega p\,, \qquad \zeta = i\,\omega\,\eta \tag{7}$$

where p and η are the horizontal and vertical slownesses, equations (3) can be rewritten as

$$s_z(r,z,t) \sim \mathrm{Re}\left\{\frac{e^{i\left(\omega t+\frac{\pi}{4}\right)}}{4\,\pi}\sqrt{\frac{2\,\omega^3}{\pi\, r}}\int_{-\infty}^{\infty}\frac{Q(p)}{\sqrt{p}}\, e^{-i\,\omega\,\eta_{qP}\,h+\omega f(p)}\; p\; dp\right\} \tag{8}$$

where

$$f(p) = -i\left(p\,r+\eta_{qS}\,z\right) = -i\,\tau(p)\ . \tag{9}$$

We use the method of the steepest descent to evaluate the integral (8) but limit ourselves to the S^* arrival, ignoring the qP-qS reflection. To achieve the goal, we distort the original path of integration away from the real axis into the complex p-plane so that a small range of p values around the saddle point $p = p_S$ contributes significantly to the integral. Around the saddle point $p = p_S$ given by

$$\frac{d\,f(p)}{d\,p} = 0 \tag{10}$$

or

$$-\frac{d\,\eta_{qS}(p)}{d\,p}\bigg|_{p=p_s} = -\,\eta'_{qS}(p)\,\big|_{p=p_s} = \frac{r}{z} = \tan\phi \tag{11}$$

where ϕ is the ray angle (Figure 2), the integrand except $e^{\,\omega f(p)}$ varies much slowly and therefore can be approximated by its value at $p = p_S$, i.e.,

$$s_z(r,z,t) \sim \mathrm{Re}\left\{\frac{e^{i\left(\omega t+\frac{\pi}{4}\right)}}{4\,\pi}\sqrt{\frac{2\,\omega^3}{\pi\, r}}\left[\frac{Q(p)}{\sqrt{p}}\, e^{-i\,\omega\,\eta_{qP}\,h}\; p\right]_{p=p_S}\int_{\Omega} e^{\,\omega f(p)}\, dp\right\} \tag{12}$$

where Ω is the distorted complex path of integration (see e.g. Daley and Hron, 1983a for isotropic case). It is also true that $e^{-i\omega\eta_{qP}h}$ is a decreasing exponential with depth h since $1/c_{qP} < p_s < 1/c_{qS}$ and $\mathrm{Im}\left(\zeta_{qP}\right) < 0$ where c is the phase velocity. Near $p = p_S$, one can write

$$p - p_s = \varepsilon e^{i\chi} \quad \text{for } -\infty < \varepsilon < \infty \tag{13}$$

and

$$f(p) \sim f(p_s) + \frac{1}{2} f''(p_s)\, \varepsilon^2 e^{2i\chi} \,. \tag{14}$$

In terms of ε,

$$s_z(r,z,t) \sim \mathrm{Re}\left\{ \frac{e^{i\left(\omega t + \frac{\pi}{4}\right)}}{4\pi} \sqrt{\frac{2\omega^3}{\pi r}} \left[\frac{Q(p)}{\sqrt{p}} e^{-i\omega\{\eta_{qP}h + \tau(p)\}}\, p \right]_{p=p_S} \int_{-\infty}^{\infty} e^{\psi(p_s)\varepsilon^2 + i\chi}\, d\varepsilon \right\} \tag{15}$$

where

$$\psi(p) = \frac{\omega}{2} f''(p)\, e^{2i\chi} \,. \tag{16}$$

Following DeSanto (1992), expression (15) can be simplified as

$$s_z(r,z,t) \sim \mathrm{Re}\left\{ \frac{\omega e^{i\omega t}\, e^{i\{\mathrm{sgn}[\mathrm{Im}(f''(p_s))]+1\}\frac{\pi}{4}}}{2\pi} \frac{1}{\sqrt{r}} \left[\frac{Q(p)}{\sqrt{p}} e^{-i\omega\{\eta_{qP}h + \tau(p)\}} \sqrt{\frac{|\mathrm{Im}[f''(p)]|}{|f''(p)|^2}}\, p \right]_{p=p} \right\} \tag{17}$$

where the sign function is used :

$$\mathrm{sgn}(x) = \begin{cases} 1 & \text{for } x > 0 \\ -1 & \text{for } x < 0 \end{cases} \tag{18}$$

provided that

$$\tan(2\chi_s) = -\frac{\mathrm{Im}[f''(p_s)]}{\mathrm{Re}[f''(p_s)]} \tag{19}$$

which makes $\mathrm{Im}[\psi(p_s)]$ vanish. Making use of the relation

$$r = R\sin(\phi) \quad \text{and} \quad z = R\cos(\phi), \tag{20}$$

with $R = \sqrt{r^2 + z^2}$, we obtain the following asymptotic expressions for the S^* arrival

$$s_z(r,z,t) \sim \frac{\omega}{\sqrt{2}\,\pi}\,\mathrm{Re}\left\{\Psi(p_s)\,\frac{e^{i\omega[t-\tau(p_s)]}}{R}\,p_s\right\} \tag{21}$$

where

$$\Psi(p) = \frac{1}{\sqrt{\sin(2\phi)}}\,\frac{Q(p)}{\sqrt{p}}\,e^{-i\omega\eta_{qP}h}\,e^{i\{\mathrm{sgn}[\mathrm{Im}(e^{-i\pi/2}\eta''_{qS})]+1\}\frac{\pi}{4}}\sqrt{\frac{|\,\mathrm{Im}[e^{-i\pi/2}\eta''_{qS}]\,|}{|\,\eta''_{qS}\,|^2}} \tag{22}$$

Similarly, the horizontal displacement can be easily obtained by taking the differentiation of the asymptotic expression

$$s_z(r,z,t) \sim \frac{1}{\sqrt{2}\,\pi}\,\mathrm{Re}\left\{\Psi(p_s)\,\frac{\tilde{B}}{p_s\,\eta_{qS}}\,\frac{\partial}{\partial r}\,\frac{e^{i\omega[t-\tau(p_s)]}}{R}\right\} \tag{23}$$

where

$$\tilde{B} = \frac{\rho - p^2 L - C\,\eta_{qS}^2}{(F + L)}\,. \tag{24}$$

Thus

$$s_r(r,z,t) \sim -\frac{\omega}{\sqrt{2\,\pi}}\,\mathrm{Re}\left\{\Psi(p_s)\,\frac{e^{i\omega[t-\tau(p_s)]}}{R}\,\frac{\tilde{B}}{\eta_{qS}} + O\left(R^{-2}\right)\right\}\,. \tag{25}$$

CONCLUSIONS

We applied the wavenumber-frequency *(ω-k)* technique to compute full-wave synthetic seismograms for a homogeneous transversely-isotropic half-space. The method has the merit of producing complete seismograms including geometrical and nongeometrical arrivals for a particular model. The source is either a vertical point force or an explosive point source. Numerical simulation for two anisotropic solids demonstrated the existence of the nongeometrical *S** arrival. However, the less anisotropic half-space generates much stronger *S** wave. This seems to suggest, inconclusively in this paper, that isotropy produces the strongest nongeometrical *S** arrival.

ACKNOWLEDGMENTS

This research was supported by NSERC, the University of Calgary and the Consortium for Research in Elastic Wave Exploration Seismology (the CREWES project). We would like to thank Prof. F. Abramovici for allowing us to quote and use two explicit expressions for an explosive source from his preprint.

REFERENCES

Abramovici, F., and L. H. T. Le. (1993), Defining an explosive point-source in a transversely isotropic medium, the CREWES report, the University of Calgary.

Abramovici, F. (1992), The double integral solution of seismic problems, J. Geophys. Res. 97, 3431-3441.

Abramovici, F., L. H. T. Le, and E. R. Kanasewich. (1989), The evanescent wave in Cagniard's problem for a line source generating SH waves, Bull. Seism. Soc. Am. 79, 1941-1955.

Abramowitz, M., and I. A. Stegun., Handbook of Mathematical Functions (U. S. National Bureau of Standards, Washington, D. C. 1972).

Backus, G. E. (1962), Long-wave elastic anisotropy produced by horizontal layering, J. Geophys. Res. 67, 4427-4440.

Berryman, J. G. (1979), Long-wave elastic anisotropy in transversely isotropic media, Geophysics 44, 896-917.

Byun, B. S. (1984), Seismic parameters for transversely isotropic media, Geophysics 49, 1908-1914.

Carcione, J. M. (1992), Anisotropic Q and velocity dispersion of finely layered media, Geophys. Prosp. 40, 761-783.
Crampin, S., and D. B. Taylor. (1971), The propagation of surface waves in anisotropic media, Geophys. J. R. astr. Soc. 25, 71-87.
Daley, P. F., and F. Hron. (1983a), High-frequency approximation to the nongeometrical S* arrival, Bull. Seism. Soc. Am. 73, 109-123.
Daley, P. F., and F. Hron. (1983b), Nongeometric arrivals due to highly concentrated sources adjacent to plane interfaces, Bull. Seism. Soc. Am. 73, 1655-1671.
Daley, P. F., and F. Hron. (1977), Reflection and transmission coefficients for transversely isotropic media, Bull. Seism. Soc. Am. 67, 661-675.
DeSanto, J. A., Scalar Wave Theory (Springer-Verlag, New York 1992) p. 137-141.
Gutowski, P. R., F. Hron, D. E. Wagner, and S. Treitel. (1984), S*, Bull. Seism. Soc. Am. 74, 61-78.
Helbig, K. (1984), Transverse isotropy in exploration seismics, Geophys. J. R. astr. Soc. 76, 79-88.
Hron, F., and B. G. Mikhailenko. (1981), Numerical modeling of nongeometrical effects by the Alekseev-Mikhailenko method, Bull. Seism. Soc. Am. 71, 1011-1029.
Kim, J. Y., and J. Behrens. (1986), Experimental evidence of S* wave, Geophys. Prosp. 34, 100-108.
Krebes, E. S., and L. H. T. Le. (1993), Plane and cylindrical SH waves in anisotropic anelastic media, submitted to J. Geophys. Res.
Levin, F. K. (1989), SV-wave velocities from P-P and P-SV data for transversely isotropic solids, Geophysics 54, 1336-1338.
Mallick, S. and L. N. Frazer (1987), Practical aspects of reflectivity modeling, Geophysics 52, 1355-1364.
Martynov, V. N. and B. G. Mikhailenko. (1984), Numerical modeling of propagation of elastic waves in anisotropic inhomogeneous media for the half-space and the sphere, Geophys. J. R. astr. Soc. 76, 53-63.
Postma, G. W. (1955), Wave propagation in a stratified medium, Geophysics 20, 780-806.
Schoenberg, M. (1993), Isotropic constituent layers equivalent to a transversely isotropic medium, EAEG- 55th meeting and technical exhibition, Stavanger, Norway, June 7-11.
Slater, C., S. Crampin, L. Y. Brodov and V. M. Kuznetsov (1993), Observations of anisotropic cusps in transversely isotropic clay, Can. J. Expl. Geophys. 29, 216-226.
Sprenke, K. F. and E. R. Kanasewich. (1977), Synthetic seismograms and the response of an anisotropic attenuating medium, Can. J. Earth Sci. 14, 1062-1076.
Stoneley, R. (1949), Seismological implications of aeolotropy in continental structure, Monthly Notices of the Roy. Astr. Soc. 5, 343-353.
Uhrig, L. F. and F. A. Van Melle. (1955), Velocity anisotropy in stratified media, Geophysics 20, 774-779.
White, J. E., L. Martineau-Nicoletis and C. Monash. (1983), Measured anisotropy in Pierre Shale, Geophys. Prosp. 31, 709-725.
White, J. E. (1982), Computed waveforms in transversely isotropic media, Geophysics 47, 771-783.

APPENDIX A : COMPLETE SOLUTIONS FOR A BURIED SOURCE IN A HALF-SPACE

The problem was formulated in the *wavenumber-frequency* space where we seek the displacement-stress vectors describing the wavefields in a homogeneous transversely isotropic (TI) solid with a vertical axis of symmetry coinciding with the z-axis (Fig. 2). Since cylindrical symmetry is assumed for the medium and the source, the transformed displacement-stress vector $\mathbf{u} = [\, w(z), q(z); W(z), Q(z) \,]^T$ in $(\omega\text{-}k)$ space where T is the transpose of a vector are :

$$(\mathbf{u}_{qP})_{\pm} = \begin{pmatrix} \pm \zeta_{qP} \\ \dfrac{B_{qP}}{k} \\ C_{qP} \\ \pm \dfrac{D_{qP}\, \zeta_{qP}}{k} \end{pmatrix} e^{\pm \zeta_{qP} z} \quad \text{and} \quad (\mathbf{u}_{qS})_{\pm} = \begin{pmatrix} k \\ \pm \dfrac{B_{qS}}{\zeta_{qS}} \\ \pm \dfrac{C_{qS}\, k}{\zeta_{qS}} \\ D_{qS} \end{pmatrix} e^{\pm \zeta_{qS} z} \tag{A.1}$$

where the subscripts qP and qS denote quasi-compressional and quasi-shear components of the wavefields, the *plus* and the *minus* signs describe the upgoing and downgoing wavefields respectively,

$$B_{qP} = \frac{\rho\,\omega^2 - k^2 L + C\,(\zeta_{qP})^2}{F + L}\,, \qquad B_{qS} = \frac{\rho\,\omega^2 - k^2 L + C\,(\zeta_{qS})^2}{F + L}\,,$$

$$C_{qP} = \frac{-F\,(\rho\,\omega^2 - k^2 L) + L\,C\,(\zeta_{qP})^2}{F + L}\,, \qquad C_{qS} = \frac{-F\,(\rho\,\omega^2 - k^2 L) + L\,C\,(\zeta_{qS})^2}{F + L}\,,$$

$$D_{qP} = \frac{L\left[\,\rho\,\omega^2 + k^2 F + C\,(\zeta_{qP})^2\,\right]}{F + L} \quad \text{and} \quad D_{qS} = \frac{L\left[\,\rho\,\omega^2 + k^2 F + C\,(\zeta_{qS})^2\,\right]}{F + L}\,. \tag{A.2}$$

The quasi-eigenvalues ζ_{qP} and ζ_{qS} are given by

$$\zeta_{qP} = \frac{\sqrt{2}}{2}\left(X + \sqrt{X^2 + Y}\right)^{1/2} \tag{A.3}$$

and

$$\zeta_{qS} = \frac{\sqrt{2}}{2}\left(X - \sqrt{X^2 + Y}\right)^{1/2} \tag{A.4}$$

where

$$X = \frac{A}{L}\left(k^2 - \frac{\omega^2 \rho}{A}\right) + \frac{L}{C}\left(k^2 - \frac{\omega^2 \rho}{L}\right) - k^2 \frac{(F+L)^2}{C\,L} \quad , \tag{A.5}$$

$$Y = -4\,\frac{A}{C}\left(k^2 - \frac{\omega^2 \rho}{A}\right)\left(k^2 - \frac{\omega^2 \rho}{L}\right) \tag{A.6}$$

and only eigenvalues in the first quadrant of the complex ζ-plane are used to ensure radiation condition is satisfied. Note that the eigenvectors given by (A.1) govern the propagation of the wavefields in a homogeneous TI space and are determined up to a multiplicative constant. Their singularities can be removed by multiplying with k and ζ_{qS} respectively. However, the present expressions are preferred since they reduce to the isotropic eigenvectors when the elastic constants are isotropic (Abramovici, 1992).

The vertical displacement s_z and horizontal displacement s_r can be written in terms of a double Bessel-Fourier integrals:

$$s_z(r,z,t) = \frac{1}{2\,\pi^2}\,\mathrm{Re}\int_0^\infty G(\omega)\, e^{i\omega t}\, d\omega \int_0^\infty \tilde{S}_0(\omega,k,z_s)\, J_0(kr)\, k\, dk \tag{A.7}$$

and

$$s_r(r,z,t) = -\frac{1}{2\,\pi^2}\,\mathrm{Re}\int_0^\infty G(\omega)\, e^{i\omega t}\, d\omega \int_0^\infty \tilde{S}_1(\omega,k,z_s)\, J_1(kr)\, k\, dk \tag{A.8}$$

where $G(\omega)$ is the Fourier spectrum of the time dependence of a causal pulse $g(t)$, k, the horizontal wavenumber, ω, the angular frequency, J_0 and J_1, the zeroth and first order Bessel functions. The response functions $\tilde{S}_0$ and $\tilde{S}_1$ are a linear combination of the displacement components corresponding to the incident and reflected wavefields and Re(...) stands for the real part of a complex quantity. The unknown coefficients of the response functions can be determined by imposing boundary conditions on the displacement and stress components at the source level and the stress-free surface.

Depending on whether the receiver is above or below the source level ($z_s = h$), the response functions are given as follows:

$$(\tilde{S}_0)_{z<h} = a_1 \left\{ \zeta_{qP}\, e^{-\zeta_{qP}|z-h|} + \zeta_{qP}\, \boldsymbol{R}_{qPqP}\, e^{-\zeta_{qP}(z+h)} - \zeta_{qS}\, \boldsymbol{R}_{qPqS}\, e^{-\zeta_{qP}h-\zeta_{qS}z} \right\}$$

$$+ a_2 \left\{ k\, e^{-\zeta_{qS}|z-h|} + \zeta_{qP}\, \boldsymbol{R}_{qSqP}\, e^{-\zeta_{qS}h-\zeta_{qP}z} - k\, \boldsymbol{R}_{qSqS}\, e^{-\zeta_{qS}(z+h)} \right\}, \tag{A.9}$$

$$(\tilde{S}_0)_{z>h} = -a_3\, \zeta_{qP}\, e^{-\zeta_{qP}|z-h|} + a_1 \left\{ \zeta_{qP}\, \boldsymbol{R}_{qPqP}\, e^{-\zeta_{qP}(z+h)} - \zeta_{qS}\, \boldsymbol{R}_{qPqS}\, e^{-\zeta_{qP}h-\zeta_{qS}z} \right\}$$

$$+ a_4\, k\, e^{-\zeta_{qS}|z-h|} + a_2 \left\{ \zeta_{qP}\, \boldsymbol{R}_{qSqP}\, e^{-\zeta_{qS}h-\zeta_{qP}z} - k\, \boldsymbol{R}_{qSqS}\, e^{-\zeta_{qS}(z+h)} \right\}, \tag{A.10}$$

$$(\tilde{S}_1)_{z<h} = a_1 \left\{ \frac{B_{qP}}{k}\, e^{-\zeta_{qP}|z-h|} - \frac{B_{qP}}{k}\, \boldsymbol{R}_{qPqP}\, e^{-\zeta_{qP}(z+h)} + \frac{B_{qS}}{k}\, \boldsymbol{R}_{qPqS}\, e^{-\zeta_{qP}h-\zeta_{qS}z} \right\}$$

$$+ a_2 \left\{ \frac{B_{qS}}{\zeta_{qS}}\, e^{-\zeta_{qS}|z-h|} - \frac{B_{qP}}{k}\, \boldsymbol{R}_{qSqP}\, e^{-\zeta_{qS}h-\zeta_{qP}z} + \frac{B_{qS}}{\zeta_{qS}}\, \boldsymbol{R}_{qSqS}\, e^{-\zeta_{qS}(z+h)} \right\}, \tag{A.11}$$

$$(\tilde{S}_1)_{z>h} = a_3\, \frac{B_{qP}}{k}\, e^{-\zeta_{qP}|z-h|} + a_1 \left\{ -\frac{B_{qP}}{k}\, \boldsymbol{R}_{qPqP}\, e^{-\zeta_{qP}(z+h)} + \frac{B_{qS}}{k}\, \boldsymbol{R}_{qPqS}\, e^{-\zeta_{qP}h-\zeta_{qS}z} \right\}$$

$$- a_4\, \frac{B_{qS}}{\zeta_{qS}}\, e^{-\zeta_{qS}|z-h|} + a_2 \left\{ -\frac{B_{qP}}{k}\, \boldsymbol{R}_{qSqP}\, e^{-\zeta_{qS}h-\zeta_{qP}z} + \frac{B_{qS}}{\zeta_{qS}}\, \boldsymbol{R}_{qSqS}\, e^{-\zeta_{qS}(z+h)} \right\} \tag{A.12}$$

where

$$\boldsymbol{R}_{qPqP} = \frac{C_{qP}\, D_{qS}\, \zeta_{qS} + C_{qS}\, D_{qP}\, \zeta_{qP}}{C_{qP}\, D_{qS}\, \zeta_{qS} - C_{qS}\, D_{qP}\, \zeta_{qP}}, \tag{A.13}$$

$$\boldsymbol{R}_{qPqS} = \frac{2\,C_{qP}\,D_{qP}\,\zeta_{qP}}{C_{qP}\,D_{qS}\,\zeta_{qS} - C_{qS}\,D_{qP}\,\zeta_{qP}}, \tag{A.14}$$

$$\boldsymbol{R}_{qSqP} = \frac{2\,C_{qS}\,D_{qS}\,k}{C_{qP}\,D_{qS}\,\zeta_{qS} - C_{qS}\,D_{qP}\,\zeta_{qP}}, \tag{A.15}$$

$$\boldsymbol{R}_{qSqS} = \boldsymbol{R}_{qPqP} \tag{A.16}$$

and the unknown coefficients (a_1, a_2, a_3 and a_4) are determined by the source type: a vertical point force or an explosive point source.

There are six terms in Eqns (A.9)-(A.12): the first term denotes an incident *qP* arrival, the second, a reflected *qP*-*qP* arrival, the third, a converted reflected *qP*-*qS* arrival, the fourth, an incident *qS* arrival, the fifth, a converted reflected *qS*-*qP* arrival and the sixth, a reflected *qS*-*qS* arrival.

For a vertical point force, the coefficients a_1, a_2, a_3 and a_4 are

$$a_1 = -\,a_3 = f_o \frac{\rho\,\omega^2 - k^2\,L + C\left(\zeta_{qS}\right)^2}{2\,C\left(\rho\,\omega^2 - k^2\,L\right)\left[\left(\zeta_{qP}\right)^2 - \left(\zeta_{qS}\right)^2\right]} \tag{A.17}$$

and

$$a_2 = a_4 = -\,f_o \frac{\zeta_{qS}}{k} \frac{\rho\,\omega^2 - k^2\,L + C\left(\zeta_{qP}\right)^2}{2\,C\left(\rho\,\omega^2 - k^2\,L\right)\left[\left(\zeta_{qP}\right)^2 - \left(\zeta_{qS}\right)^2\right]} \tag{A.18}$$

where f_o is the force per unit area per second. For an explosive source, they are (Abramovici and Le, 1993):

$$a_1 = a_3 = \frac{f_o}{\zeta_{qP}} \frac{k^2\,(F + 2\,L) - \rho\,\omega^2 - C\,\zeta_{qS}^2}{2\,C\left(\zeta_{qP}^2 - \zeta_{qS}^2\right)} \tag{A.19}$$

and

$$a_2 = -\,a_4 = -\frac{f_o}{k} \frac{k^2\,(F + 2\,L) - \rho\,\omega^2 - C\,\zeta_{qP}^2}{2\,C\left(\zeta_{qP}^2 - \zeta_{qS}^2\right)} \tag{A.20}$$

where f_o is the strength of the source dictating the volume of the material injected per second.

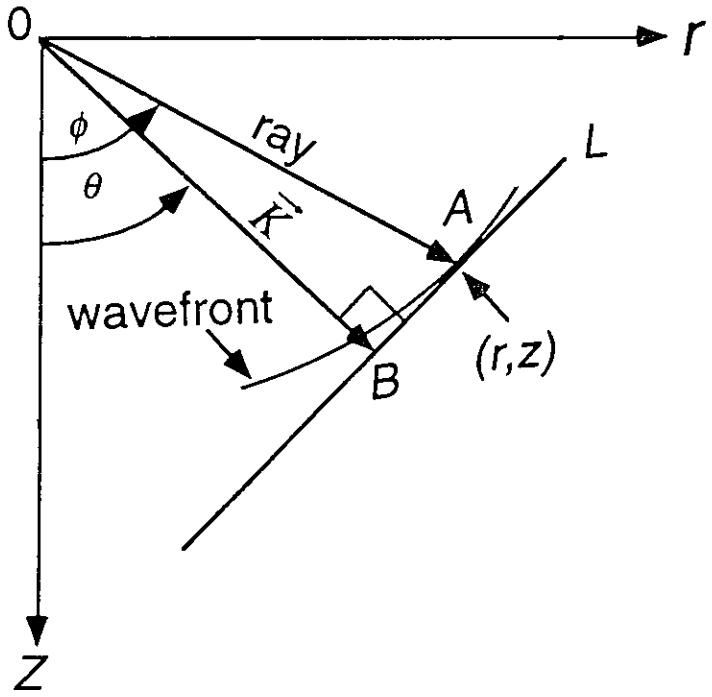

Figure 1: A schematic diagram showing the relationship between the phase and ray angles for a homogeneous transversely isotropic elastic solid. Line L is tangent to the wavefront at point A. $\overrightarrow{OA}$ denotes a ray with ray angle ϕ and $\overrightarrow{OB}$, a phase vector $\vec{K}$ with phase angle θ.

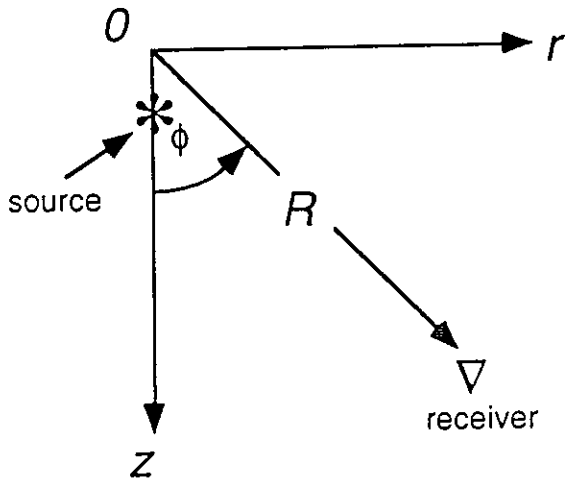

Figure 2. A buried source in a homogeneous transversely isotropic half-space. ϕ is a ray angle.

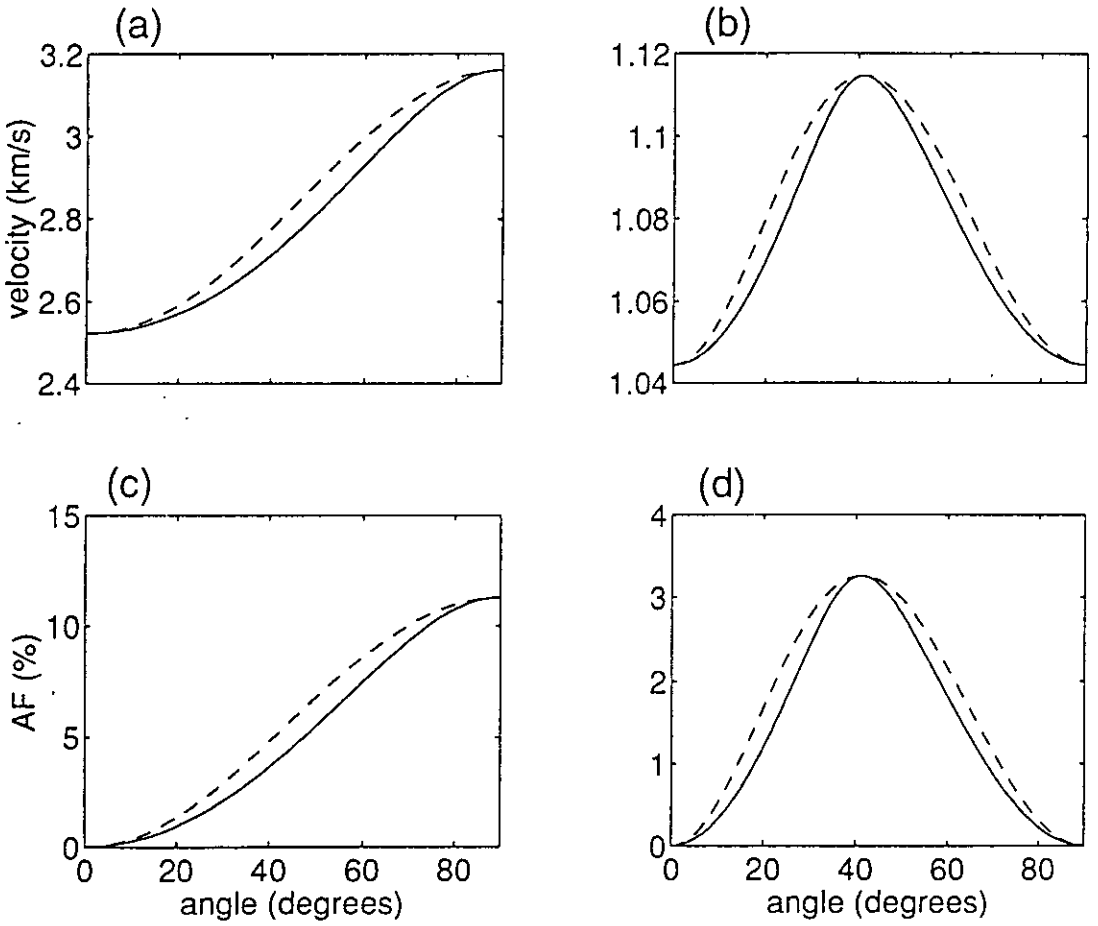

Figure 3. Phase (- - - - - -) and group (————) velocities of Austin Chalk. The parameters are $A = 22.0\text{x}10^{10}$ dynes/cm^2, $C = 14.0\text{x}10^{10}$ dynes/cm^2, $F = 12.0\text{x}10^{10}$ dynes/cm^2, $L = 2.4\text{x}10^{10}$ dynes/cm^2 and $\rho = 2.2$ g/cm^3. (a) qP wave velocity, (b) qS wave velocity, (c) anisotropy factor of qP wave and (d) anisotropy factor of qS wave. The angles are phase angles for phase velocity and group angles for group velocity accordingly.

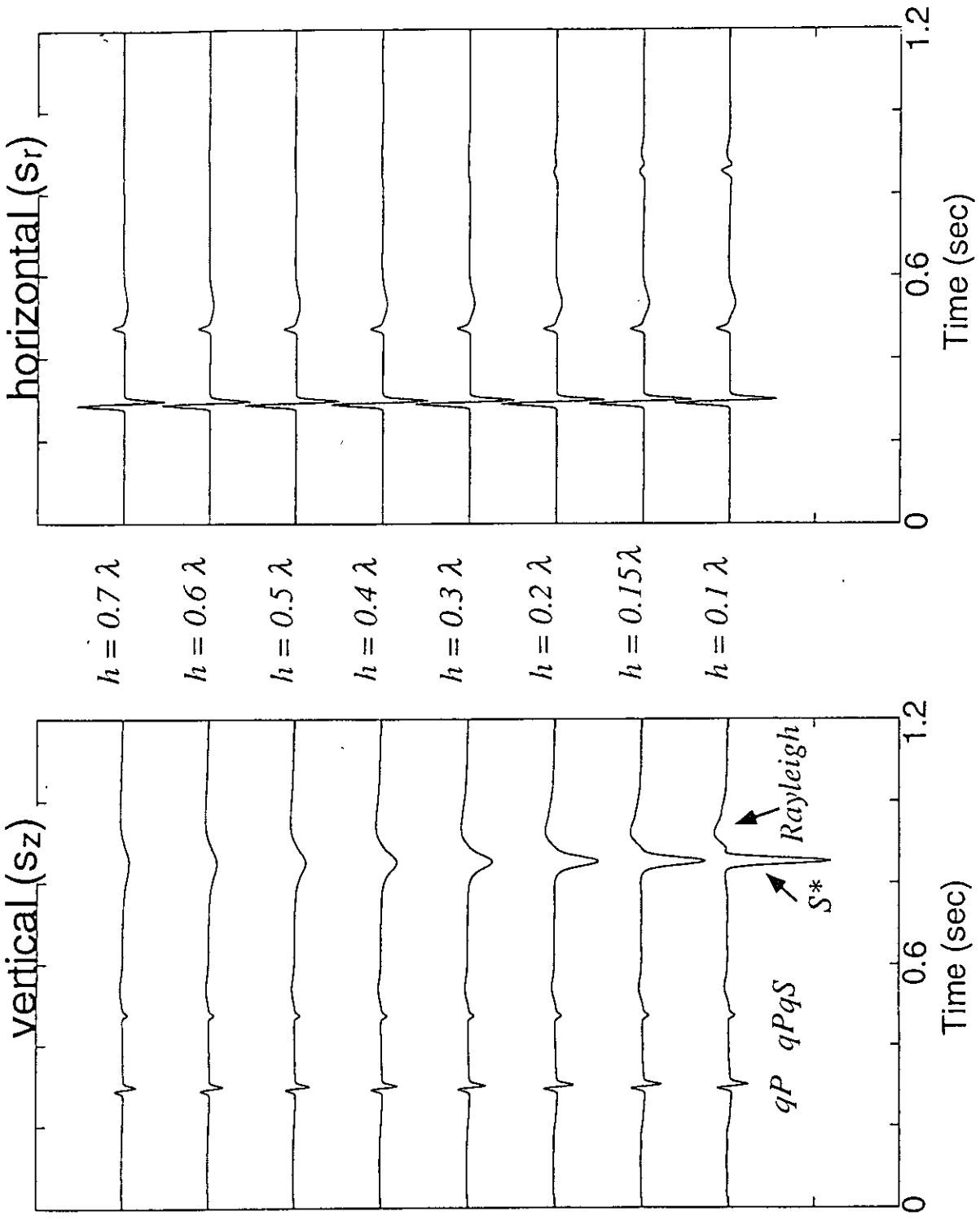

Figure 4. Synthetic displacement seismograms showing the effect of source depth on the generation of the *S** wave for a single receiver at a fixed location *(r = 12 λ and z = 3 λ)*. The source is a vertical point force. The amplitudes are scaled by a factor of 2.0E8.

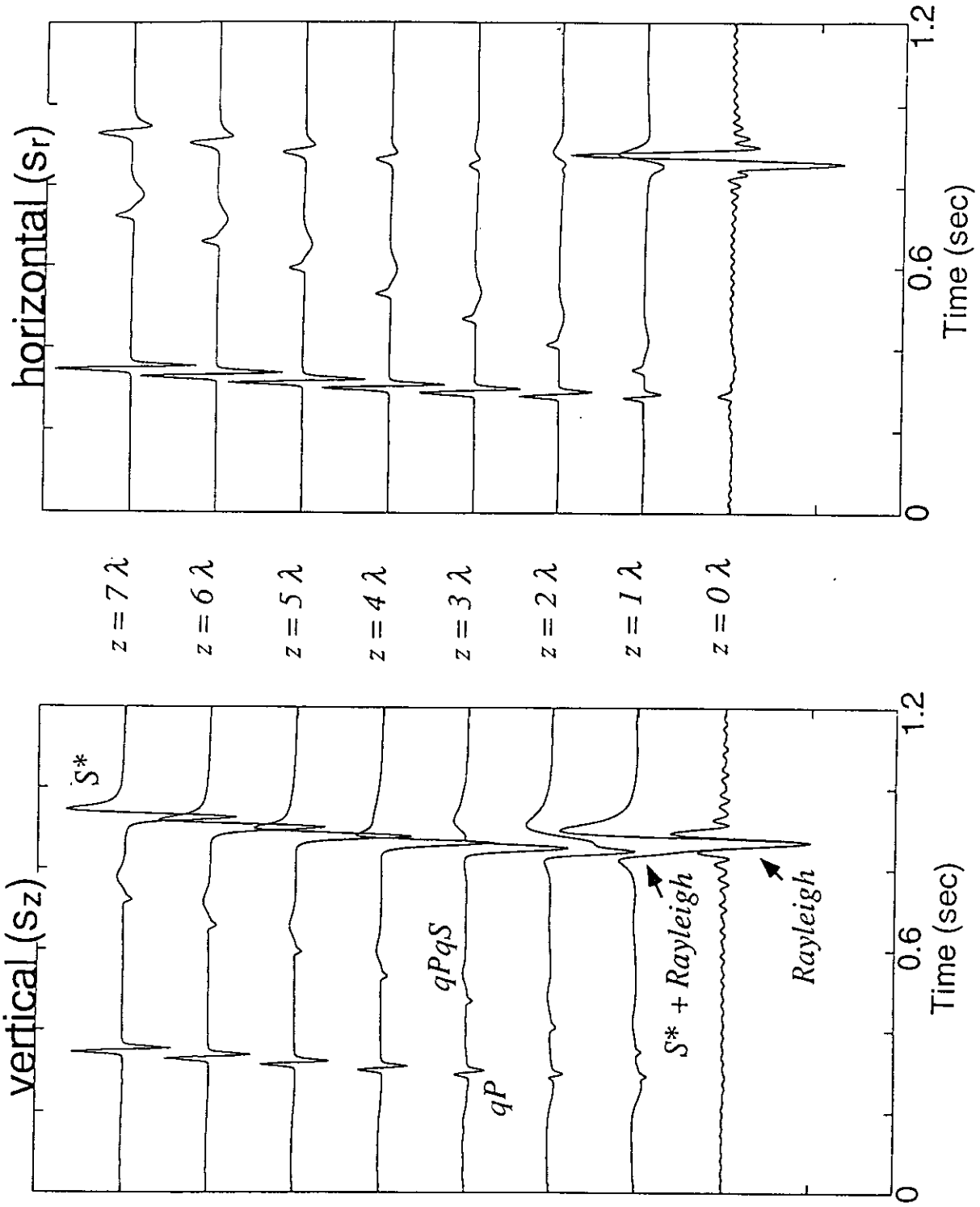

Figure 5. Synthetic displacement seismograms showing the effect of receiver depth on the amplitude of the S^* wave for a single source ($z_s = 0.1\ \lambda$) at fixed receiver offset ($r = 12\ \lambda$). The source is a vertical point force. The amplitudes are scaled by a factor of 2.0E8 except the first trace of vertical motion which is scaled by a factor of 2.0E7 for display purpose.

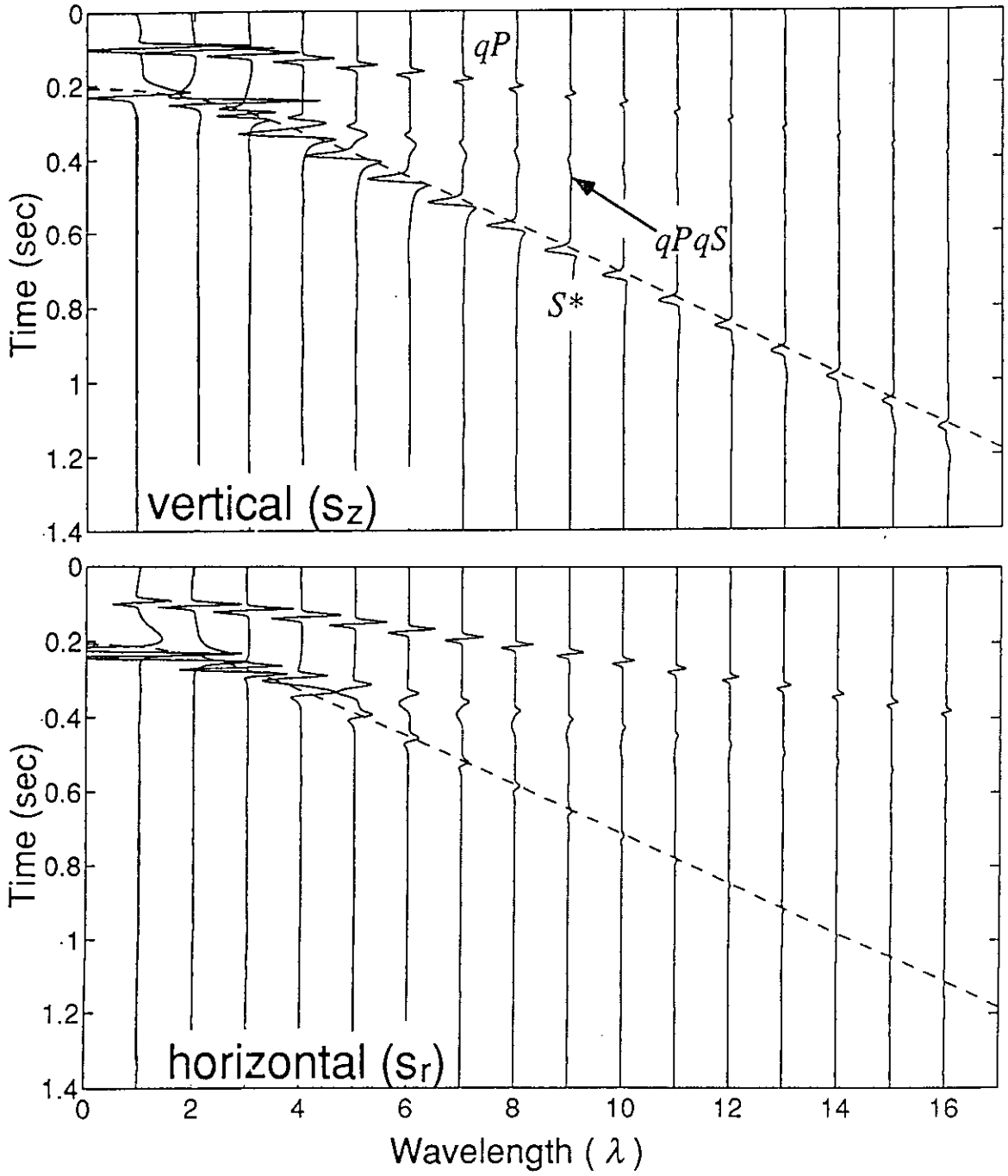

Figure 6. Synthetic displacement seismograms for a horizontal array of receivers at a depth of 3 λ with offset ranging from 1 λ to 16 λ. The source is a vertical point force buried *0.1* λ below the free surface. The amplitudes are scaled by a factor of 5.0E7. The dashed curve shows the arrival time of the direct *qS* arrival from the source.

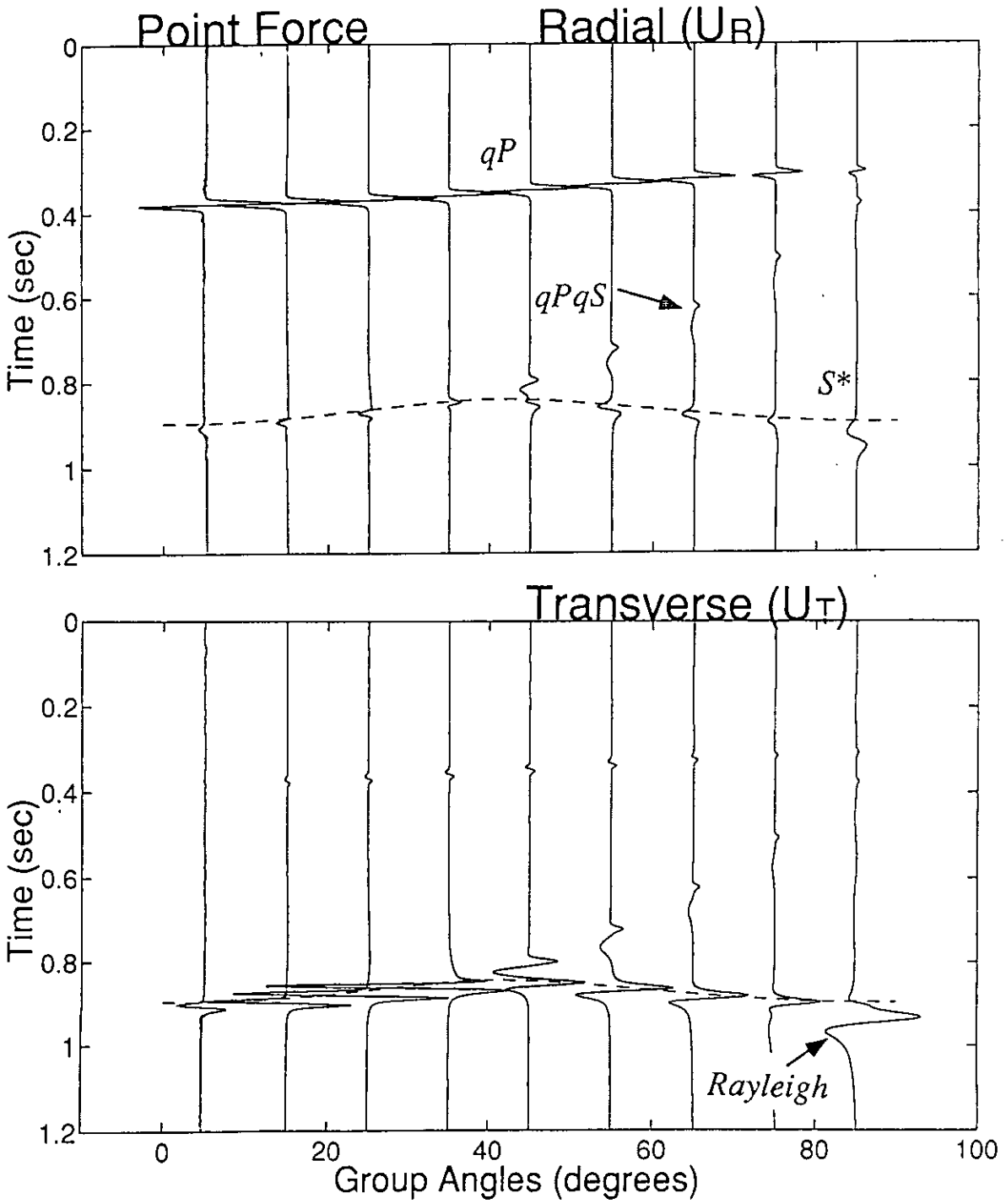

Figure 7. Synthetic radiation pattern showing the effect of direction on the generation of the S^* wave in Austin Chalk. The source is a vertical point force ($z_s = 0.1\ \lambda$). Nine receivers are placed around a circular arc with a radius of 13 λ from the source located at the center of the arc. The ray angles range from 5° to 85°. The amplitudes are scaled by a factor of 1.0E9. The dashed curve shows the arrival time of the direct qS arrival from the source.

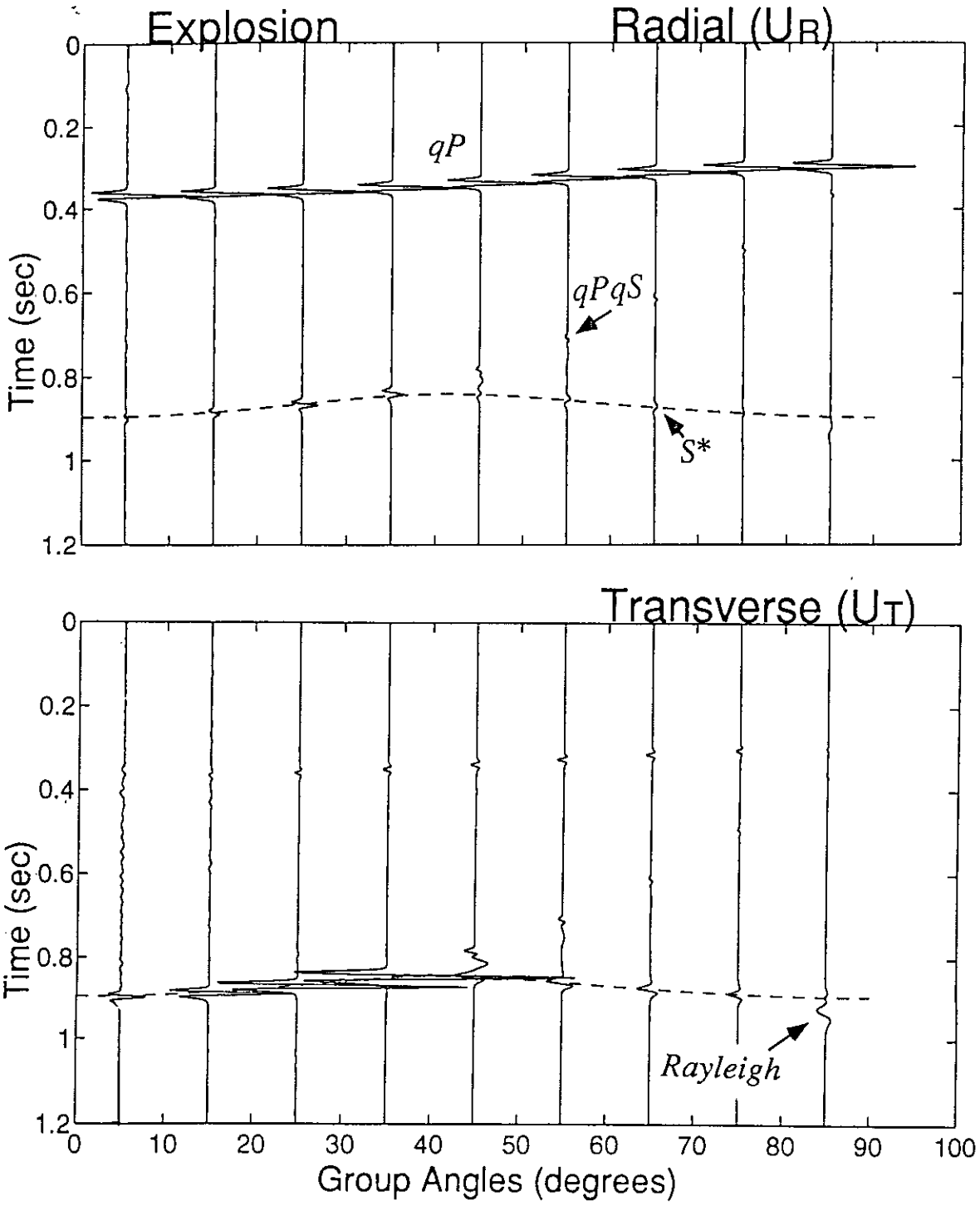

Figure 8. Synthetic radiation pattern showing the effect of direction on the generation of the S^* wave in Austin Chalk. The source is an explosive point source ($z_s = 0.1\ \lambda$). Nine receivers are placed around a circular arc with a radius of 13 λ from the source located at the center of the arc. The ray angles range from 5° to 85°. The amplitudes are scaled by a factor of 5.0E6. The dashed curve shows the arrival time of the direct *qS* arrival from the source.

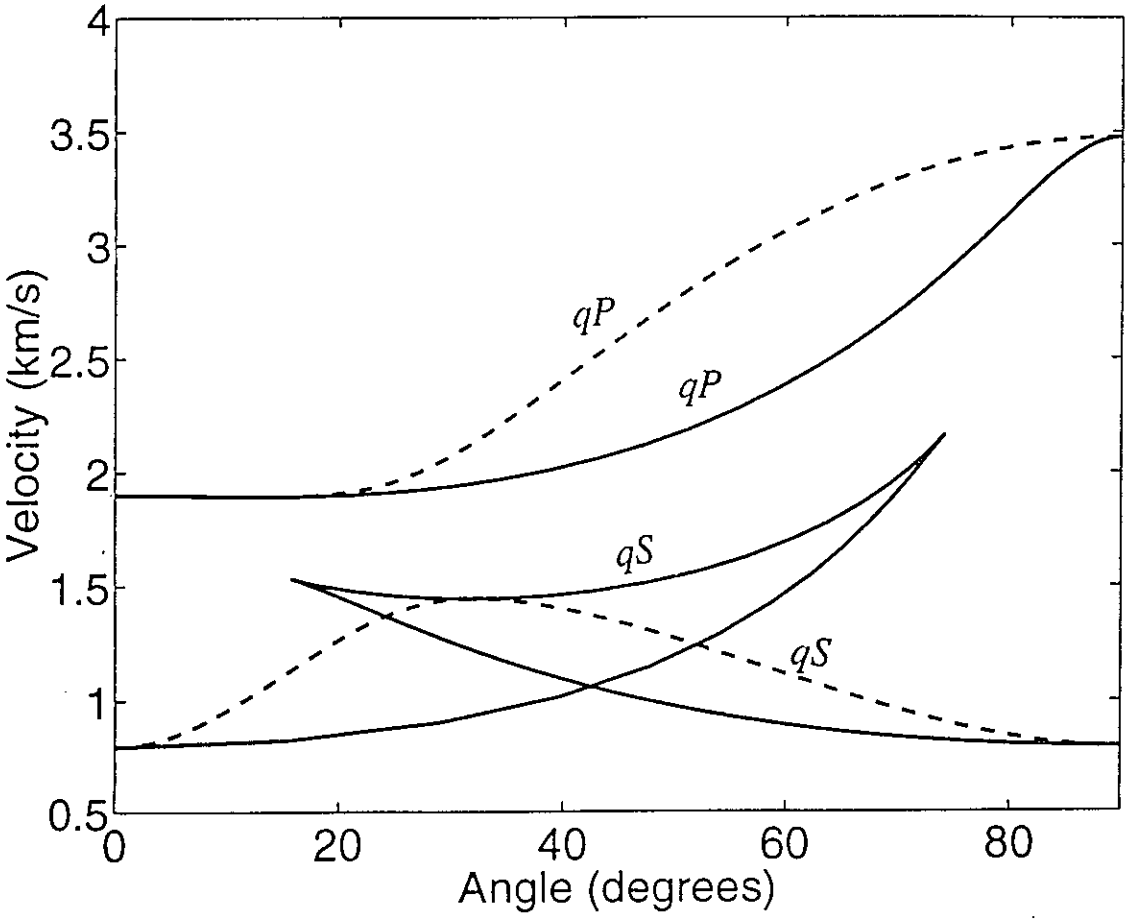

Figure 9. Phase (- - - - - -) and group (————) velocities of Gypsum Soil. The parameters are A = 28.4x10^{10} dynes/cm^2, C = 8.5x10^{10} dynes/cm^2, F = 4.3x10^{10} dynes/cm^2, L = 1.5x10^{10} dynes/cm^2 and ρ = 2.35 g/cm^3. The angles are phase angles for phase velocity and group angles for group velocity accordingly.

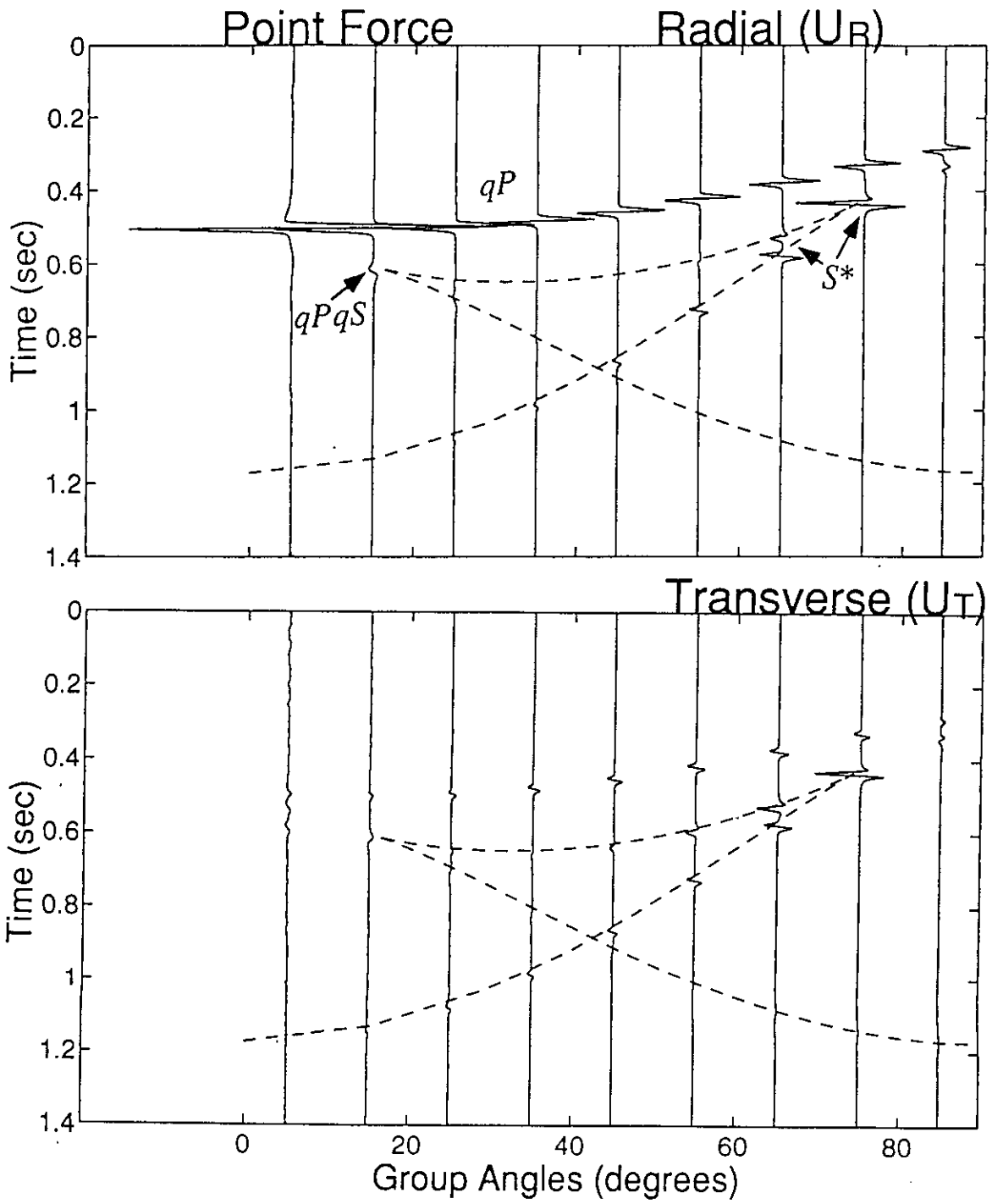

Figure 10. Synthetic radiation pattern showing the effect of direction on the generation of the S^* wave in Gypsum Soil. The source is a vertical point force ($z_s = 0.13\lambda$). Nine receivers are placed around a circular arc with a radius of 17.3 λ from the source located at the center of the arc. The ray angles range from 5° to 85°. The amplitudes are scaled by a factor of 1.0E9. The dashed curve shows the arrival time of the direct qS arrival from the source.

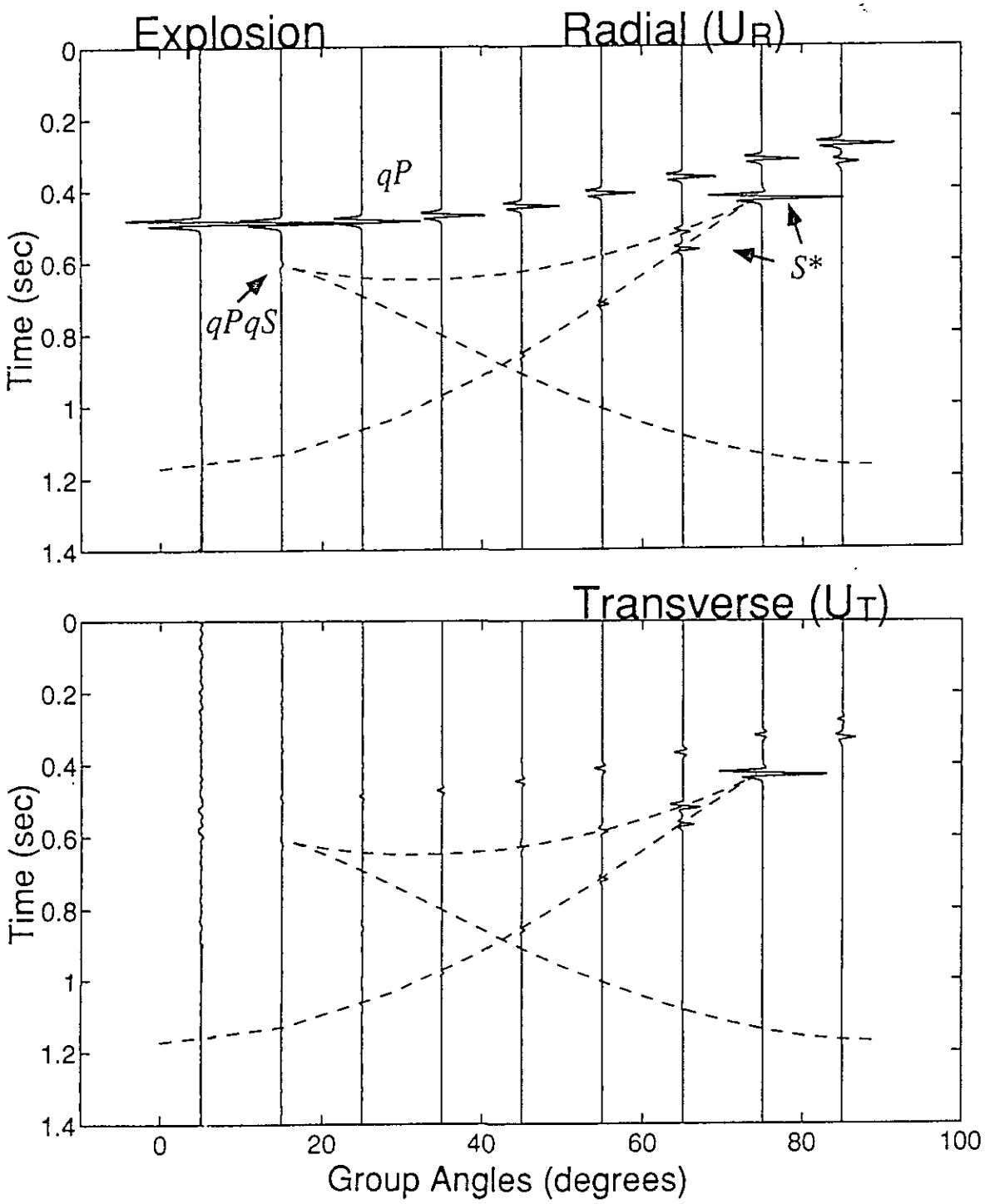

Figure 11. Synthetic radiation pattern showing the effect of direction on the generation of the S^* wave in Gypsum Soil. The source is an explosive point source ($z_s = 0.13\ \lambda$). Nine receivers are placed around a circular arc with a radius of 17.3 λ from the source located at the center of the arc. The ray angles range from 5° to 85°. The amplitudes are scaled by a factor of 5.0E6. The dashed curve shows the arrival time of the direct qS arrival from the source.